Available online at www.sciencedirect.com
SCIENCE DIRECT
Polymer 47 (2006) 826–835
polymer
www.elsevier.com/locate/polymer

Restricted chain segment mobility in poly(amide) 6/clay nanocomposites evidenced by quasi-isothermal crystallization

Hans E. Miltner [a], Guy Van Assche [a], András Pozsgay [b], Béla Pukánszky [b], Bruno Van Mele [a,*]

[a] Department of Polymer Science and Structural Chemistry, Vrije Universiteit Brussel (VUB), Pleinlaan 2, B-1050 Brussels, Belgium
[b] Department of Plastics and Rubber Technology, Budapest University of Technology and Economics, P.O. Box 91, H-1521 Budapest, Hungary

Received 21 February 2005; received in revised form 3 November 2005; accepted 5 December 2005

Abstract

Modulated temperature differential scanning calorimetry is used to explore the interactions between a poly(amide) 6 matrix and various types of clay reinforcement. During quasi-isothermal crystallization of the polymer/clay nanocomposites, an excess contribution is observed in the recorded heat capacity signal, due to reversible melting and crystallization. It is proposed that the magnitude of this excess contribution can be used to qualify the polymer/clay interfacial interaction, as it is directly linked to the segmental mobility of the polymer chains in the interphase region, where both the crystalline and amorphous polymer fractions are affected. It is shown that the interfacial interaction strongly depends on the type of clay filler used. These interactions play a key role in the development of specific material properties for the different types of nanocomposites. A simple interphase model for the poly(amide) 6/clay nanocomposites is proposed.

Keywords: Polymer/clay nanocomposites; Interphase; Modulated temperature differential scanning calorimetry

1. Introduction

In recent years, a lot of interest from both academia and industry has been attracted to the study of nanostructured materials. One particularly investigated research area deals with materials known as nanocomposites. These consist of a polymeric matrix, reinforced with a dispersed phase with at least one dimension in the range of 1–100 nm. Clay-reinforced polymers have been extensively studied. A wide range of clay materials has been investigated, with different particle sizes, different aspect ratios and changing organic treatment [1]. The latter process, resulting in an organophilic clay, has several purposes [2]. First, it leads to an increase in gallery space between individual stacked clay platelets, thus opening the gap for the penetration of polymer chains. Second, the strong interaction between clay surfaces is decreased by rendering them more organophilic. This also facilitates the diffusion of the matrix polymer chains into the clay galleries. Third, the nature of the intercalated organic modifier can be specifically adapted to the matrix material, e.g. by introducing functional groups at the chain ends, thus fine-tuning the interfacial interaction between matrix and reinforcement.

Clay nanocomposites have been reported to show promising property enhancements compared to the unmodified polymers, at very low loading in clay (1–5 wt%) (e.g. [3] for a recent review, and references therein). These range from increased Young's modulus over better thermal stability, increased barrier properties and fire-retardancy to strong nucleating effects on the crystallization of thermoplastics. In addition, the reinforcing clay has only very little influence on the optical transparency of the materials. The material improvements have been related to the very small size of the reinforcing clay platelets on one hand, and to their large aspect ratio on the other [4]. The latter facts result in the presence of very large amounts of 'interphase' material compared to conventional (micro)-composites, provided that a good dispersion of the clay platelets can be achieved. The stability of such systems is governed by thermodynamic laws (interaction between clay, organic modifier and matrix material). 'Exfoliated' morphologies can be forced by applying high shear forces [5].

The present paper will focus on the in situ monitoring of the quasi-isothermal crystallization of clay nanocomposites based on a poly(amide) 6 matrix and different organophilic montmorillonite reinforcements. These thermal properties, in

* Corresponding author. Address: Department of Polymer Science and Structural Chemistry-POSC (TW), Faculty of Applied Sciences, Vrije Universiteit Brussel (VUB), Pleinlaan 2, B-1050 Brussels, Belgium. Tel.: +32 2 629 32 76/32 88; fax: +32 2 629 32 78.
E-mail address: bvmele@vub.ac.be (B.V. Mele).

0032-3861/$ - see front matter © 2005 Elsevier Ltd. All rights reserved.
doi:10.1016/j.polymer.2005.12.014

combination with the melting and glass transition region, will be investigated by means of modulated temperature differential scanning calorimetry (MTDSC). The materials discussed have already been the subject of an extensive study with respect to mechanical properties [6].

In the study of polymer materials by means of MTDSC, the kinetics of thermal processes, depending on time and absolute temperature, often appear in the 'non-reversing' heat flow, while the (specific) heat capacity is found in the 'reversing' heat flow. The former signal equals the total heat flow (the running average of the modulated signal) minus the reversing heat flow. A complete description of the extraction of the heat capacity and other MTDSC signals can be found in literature [7,8].

The straightforward distinction of heat capacity and thermal transformations in separate MTDSC signals is no longer valid in case of polymer melting or phase separation in polymer blends and solutions. Heat effects, coupled with melting/crystallization [9,10] or mixing/demixing [11–15] can occur during one modulation cycle and thus contribute to the heat capacity signal. Hence, the heat capacity signal is termed 'apparent' heat capacity, C_p^{app}, to distinguish it from the baseline heat capacity based on thermodynamics, C_p^{base}, which is temperature-dependent. The so-called 'excess' contribution, C_p^{excess}, is temperature and time-dependent and changes with the progress of the transformation:

$$C_p^{app}(T,t) = C_p^{base}(T) + C_p^{excess}(T,t)$$

The origin, magnitude and time-dependency of C_p^{excess} for the poly(amide) 6/clay nanocomposites will be related to melting/crystallization processes in the interphase region between polymeric matrix and inorganic reinforcement. In case of a transformation from the molten to the semi-crystalline state at temperature T, C_p^{base} also depends on the isothermal crystallization time t, due to the change of crystallinity in the nanocomposite.

2. Experimental

2.1. Materials and sample preparation

The poly(amide) 6 used as matrix in this study is dynamid E grade poly(caprolactam) produced by Zoltek Rt., Hungary. Two organophilic clays with different organic modifiers or surfactants have been used: Nanofil 784 organophilized with ω-aminolauric acid for strong interfacial interaction (termed 'acid'), and Nanofil 948 treated with dimethyldistearylamine, which is expected to decrease the strength of interfacial adhesion (termed 'aliphatic'). Both layered silicates were supplied by Süd-Chemie AG, Germany. For comparison, an unmodified bentonite clay was used (Majorbenton B, termed 'neat'). Nanocomposites with filler content up to 10 vol.% and with different organic treatments were prepared by homogenization using a Rheomex S ¾″ single screw extruder driven by a Haake Rheocord EU 10V unit [6]. All samples were dried in a vacuum oven prior to measurement.

2.2. Techniques and methodology

Morphological information was gathered from WAXS experiments using a Siemens D5000 equipment with Cu K_α radiation, operating at 40 kV and 40 mA. Degrees of crystallinity were calculated according to the standard procedure using Gaussian deconvolution of the scattering peaks and of the amorphous fraction in the WAXS pattern.

The thermal properties of the nanocomposites were investigated using modulated temperature differential scanning calorimetry (MTDSC).

The quasi-isothermal MTDSC experiments were performed on a TA Instruments Q1000 (T-zero™ DSC-technology) with an RCS cooling accessory. Helium was used as a purge gas (25 ml/min). Indium was used for both temperature and enthalpy calibration.

Data are expressed as specific heat capacities or specific heat flows (or changes thereof) in J/g °C or W/g, respectively, and always on polymer basis.

Unless stated otherwise, the modulation conditions were an amplitude of 0.5 °C and a period of 60 s.

Non-isothermal MTDSC measurements were performed on a TA Instruments 2920 DSC with the MDSC™ option and an RCS cooling accessory. Temperature and enthalpy calibration was performed as above. Heat capacity calibration was performed with a poly(methyl methacrylate) standard, according to [11,12].

3. Results and discussion

The surface treatment of the clay will largely influence the nanocomposite structure and morphology, as well as its properties [16]. Clays with two different organic modifiers have been added to the poly(amide) 6 matrix to investigate the role of the surfactant: one consisting of two non-polar aliphatic chains, and the other of one shorter aliphatic chain, functionalized by a carboxylic acid end-group to interact with the poly(amide) 6. In both cases an ammonium end-group is responsible for the interaction with the clay. Based on WAXS and TEM data, exfoliation is only noticed for the lowest clay loadings. With increasing clay loading, the morphology becomes progressively more intercalated for all nanocomposites.

3.1. Crystalline structure and glass transition of poly(amide) 6/clay nanocomposites

3.1.1. Melting region

Poly(amide) 6 usually crystallizes in the α-form, with antiparallel polymer chains in planar zig-zag conformation ([17,18] p. 111). Planar sheets of hydrogen-bonded macromolecules are formed, which, in turn, are stacked in a monoclinic crystal structure. The second stable crystal form is the γ-form, in which hydrogen bonds are formed between parallel poly(amide) chains, requiring the amide linkages to twist out of the plane of the macromolecular sheets, in a way that all the hydrogen bonds can form without strain. The resulting crystal

structure is pseudo-hexagonal ([18] p. 115). The γ-crystalline phase has been found in the skin region of injection molded poly(amide) 6, subjected to rapid cooling [17]. Its formation has been proven to be favored in situations of limited chain mobility [19]. It has been advanced that unfolded polymer chains are ordered within the γ-crystals, formed in conditions where the ability for chain folding is reduced [20].

It has been reported that the presence of clay also results in a modification of the crystalline structure of poly(amide) 6, with γ-type crystals favored over the α-modification [21]. The presence of clay platelets weakens hydrogen bonding in poly(amide) 6 [22] or forces the hydrogen bonds out of the plane of the macromolecular sheets [23].

Extensive studies have been published on the non-isothermal crystallization behavior of poly(amide) 6/clay nanocomposites. On one hand, clay particles have a nucleating effect on polymer crystallization [17,24]. On the other hand, crystal growth is believed to slow down due to mobility restrictions of the macromolecular chains in the vicinity of the (organo)clay [17,19].

MTDSC thermograms of the melting region after a non-isothermal crystallization of poly(amide) 6 in the clay nanocomposites of this work are shown in Fig. 1. The presence of γ-type crystals is clearly demonstrated. A cooling rate as low as 1 °C/min was applied in order to obtain a crystal structure close to the thermodynamically stable one. After this slow cooling, heating experiments were performed at the same rate. The melting of α-type crystals, typically formed after a crystallization at low cooling rate, is seen for unfilled poly(amide) 6. Recrystallization phenomena can be observed, which partly explain the complexity of the MTDSC traces. An additional melting peak at lower temperature (212–215 °C) appears in the melting region of all nanocomposites, which is absent in the unfilled poly(amide) 6. This endothermic peak has been assigned to the melting of γ-type crystals [25,26]. The relative amount of the γ-crystalline fraction with respect to the higher melting α-type fraction strongly depends on surfactant type and clay loading. In acid- and aliphatic-modified nanocomposites, the γ-crystalline structure is dominant at all clay loadings studied. For the nanocomposites based on neat clay the γ-fraction is also present, but at low clay loading the α-structure is favored.

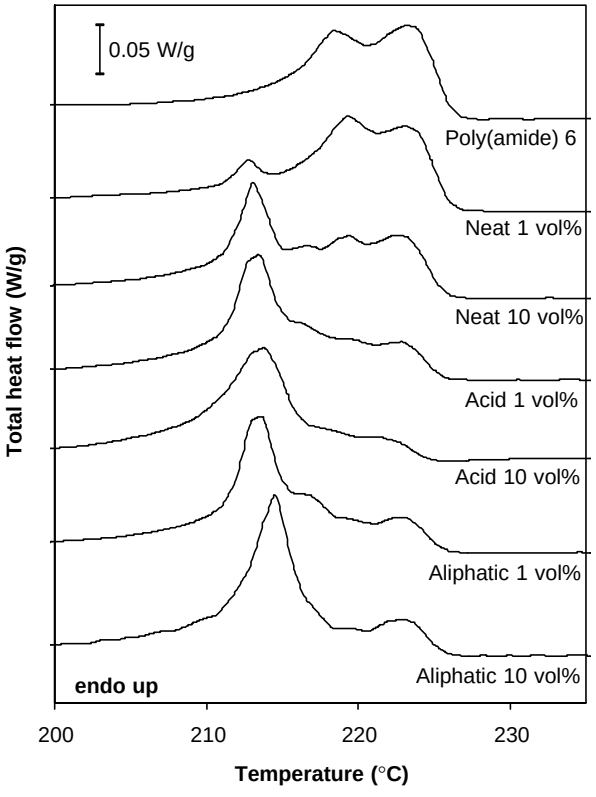

Fig. 1. Normalized total heat flow traces in the melting region of poly(amide) 6 and different nanocomposites (MTDSC at 1 °C/min; shifted vertically for clarity).

The (quasi)-isothermal crystallization behavior of poly (amide) 6 nanocomposites is further worked out in this paper.

3.1.2. Glass transition region

A lot of controversy exists on the glass transition region of polymer/clay nanocomposites. An increase in T_g or the creation of a new glass transition at higher temperature (similar to a rigid amorphous fraction) can be expected as the result of confinement effects and strong interactions between polymer and filler particles [27,28]. These interactions, leading to restricted segmental mobility of the macromolecular chains in the vicinity of the (organo)clay, retard the cooperative motions of polymer chains and increase the glass transition temperature of at least part of the polymeric material. Such mobility restrictions have been reported for amorphous poly(styrene) nanocomposites [29].

On the other hand, the absence of chain entanglements and the presence of excess free volume associated with the packing constraints of intercalated chains have been reported for poly(ethylene oxide) [30]. This would lead to a decreased T_g. Even the occurrence of non-cooperative motions, which are not traditionally associated with the glass transition, has been advanced for intercalated poly(ethylene oxide) [27].

Fig. 2 shows the temperature-derivative of the heat capacity in the glass transition region of dried poly(amide) 6/clay nanocomposites crystallized non-isothermally from the melt. The derivative curve is more sensitive to the shape and the width of the transition. If the traces are recalculated on polymer basis to subtract the fraction of organoclay that does not participate in the process of devitrification, the area under the curve is proportional to the amount of amorphous poly(amide) 6 (i.e. ΔC_p at T_g).

The derivative curve appears as a peak which ranges over ca. 60 °C, and with T_g as the maximum (Fig. 2). Neither the position or width of T_g, nor the amount of amorphous material significantly change due to the presence of clay. The type and amount of clay clearly have a negligible or at most very limited influence on the glass transition region of poly(amide) 6.

The transition observed just below T_g of the aliphatic-treated nanocomposites stems from the melting of the modifier (see discussion on interphase model, Section 3.4.1).

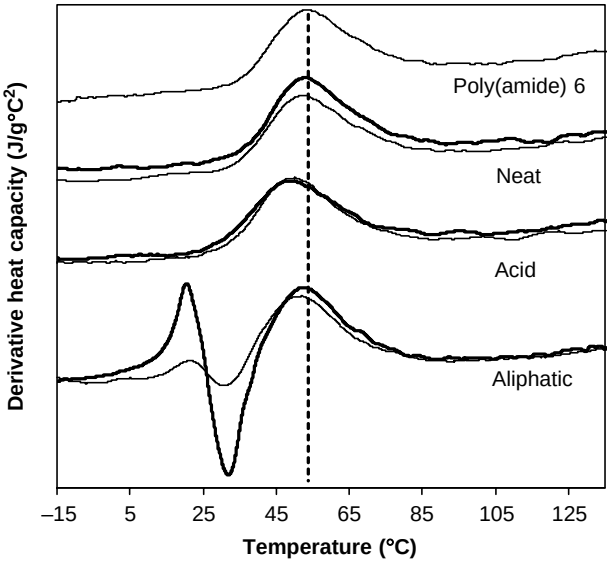

Fig. 2. Temperature-derivative of the heat capacity signal in the glass transition region of poly(amide) 6 and different nanocomposites with 1 vol.% of clay (—) and 10 vol.% of clay (—); traces are shifted vertically for clarity.

3.2. Quasi-isothermal crystallization of poly(amide) 6/clay nanocomposites

3.2.1. Melting region

The quasi-isothermal crystallization of poly(amide) 6 and its clay nanocomposites was performed at 210 °C for different periods of time using MTDSC (temperature modulation of ±0.5 °C/60 s). The melting region of the isothermally formed crystals was measured in a subsequent heating, without intermediate cooling, and their WAXS patterns were recorded. Fig. 3 shows these patterns for poly(amide) 6 and its nanocomposites crystallized at 210 °C for 1000 min. It is evidenced that γ-type crystals are found in all nanocomposite samples, to an extent depending on clay type and degree of loading.

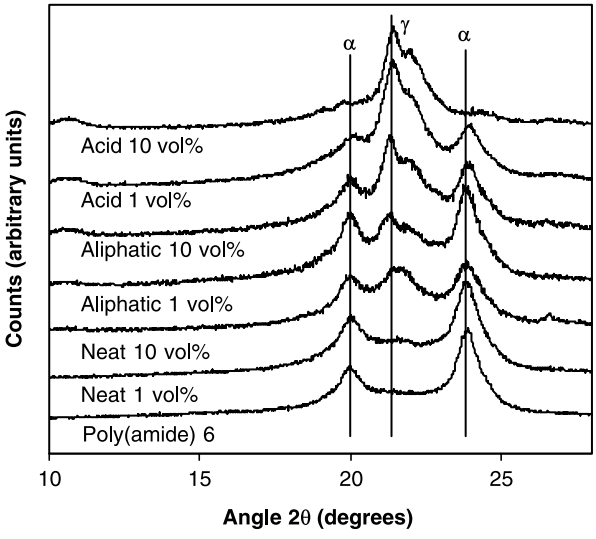

Fig. 3. WAXS patterns for poly(amide) 6 and different nanocomposites isothermally crystallized at 210 °C for 1000 min (curves shifted vertically for clarity).

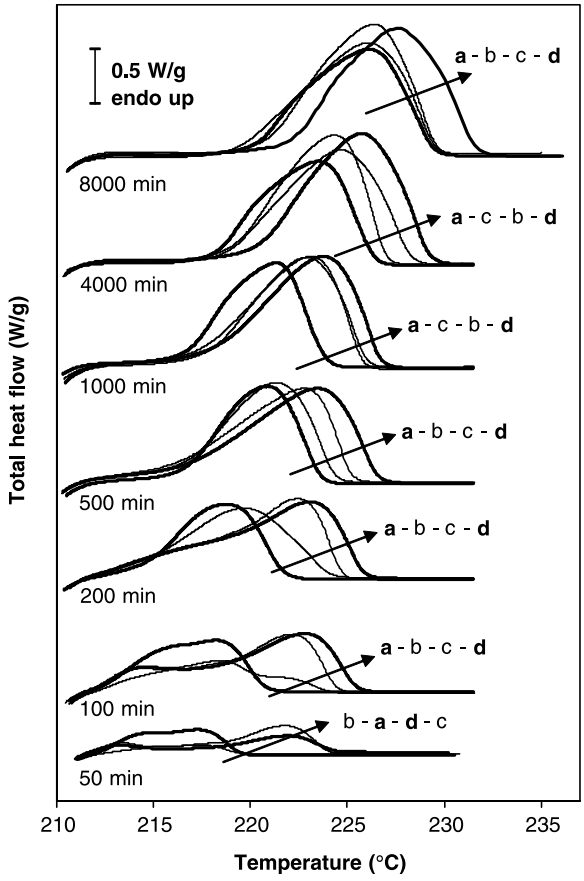

Fig. 4. Total heat flow signal (conventional DSC at 5 °C/min) in the melting region of nanocomposites containing 5 vol.% of acid (a) aliphatic (b) and neat (c) clay, and of the reference poly(amide) 6 material (d). Traces were recorded after quasi-isothermal crystallization at 210 °C for the indicated time periods.

Nanocomposites based on neat clay have a melting behavior close to that of unfilled poly(amide) 6, since they contain essentially α-crystals (Fig. 4). In contrast, nanocomposites based on acid and aliphatic clay have significantly lower melting temperatures due to the presence of γ-crystals. However, in the case of aliphatic treated clay, an important α-crystalline fraction remains present. These observations confirm the results after non-isothermal crystallization of Fig. 1.

The melting temperature increases with increasing time of quasi-isothermal crystallization (Fig. 4). This reflects an underlying process of crystal perfectioning. Fig. 5 shows that the melting enthalpy, corresponding to the traces of Fig. 4, clearly depends on the time of quasi-isothermal crystallization. If identical values for the heats of fusion of α- and γ-crystalline structures are assumed, in accordance with literature data [17], the nanocomposite based on acid clay has a ca. 25% lower crystallinity than the unfilled poly(amide) 6 after crystallization at 210 °C for 8000 min.

WAXS experiments performed after various isothermal crystallization times did not reveal a significant change in the relative amount of α- and γ-crystalline fractions. The γ-form is

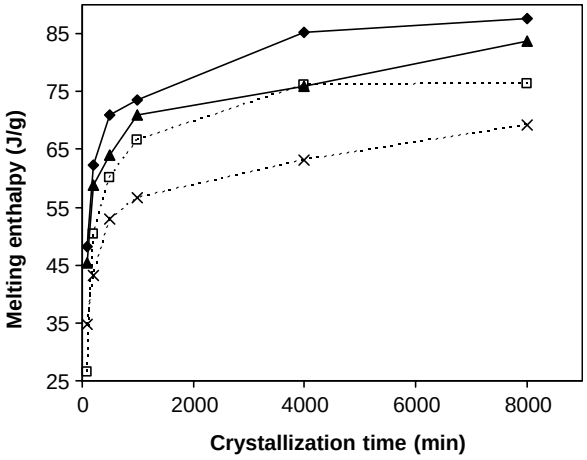

Fig. 5. Melting enthalpy of poly(amide) 6 (♦) and nanocomposites with 5 vol.% of neat (▲), aliphatic (□) and acid clay (×) measured by means of conventional DSC at a heating rate of 5 °C/min after various times of quasi-isothermal crystallization at 210 °C (values on polymer basis).

already formed in the initial stage of crystallization and can be regarded as the thermodynamically stable one near the clay [31].

3.2.2. *In situ quasi-isothermal crystallization of poly(amide) 6/clay nanocomposites*

The evolution of the heat capacity signal can be used to follow in situ the quasi-isothermal crystallization process at 210 °C (temperature modulation of ±0.5 °C/60 s). The chosen conditions result in low crystallization rates, which is essential to obtain a reliable heat capacity and non-reversing heat flow signal. A typical example is shown in Fig. 6, describing the different contributions to the heat capacity for unmodified poly(amide) 6. The largest exothermic heat effect in the non-reversing heat flow due to crystallization at 210 °C is noticed in the first 100 min. If no extra heat effect is involved in the heat capacity signal, a stepwise decrease is expected depending on the crystallinity developed (C_p^{base}), as shown in the enlarged inset of Fig. 6. The heat capacity, however, increases due to a superimposed excess contribution, C_p^{excess}, and is, therefore, termed apparent heat capacity, C_p^{app}. The excess contribution is caused by heat effects associated with 'fast' kinetic processes taking place on the timescale of the temperature modulation, i.e. excess heat of melting and crystallization, superimposed on the modulated heat flow associated with C_p^{base} (see also time domain analysis).

The evolution of C_p^{base} in the early stages of crystallization is estimated from the partial integration of the exothermicity in the non-reversing heat flow signal. The degree of crystallinity has been calculated using a literature value of 190 J/g for 100% crystalline poly(amide) 6 [32]. The limiting values of C_p^{base} of the melt (0% crystalline) and of 100% crystalline poly(amide) 6 are estimated from a linear extrapolation of the temperature-dependent heat capacity in the melt and in the glassy state. The latter provides a fair approximation of the heat capacity of the 100% crystalline state. Note that the final value of C_p^{base} drawn in Fig. 6 should not be considered as an equilibrium value of

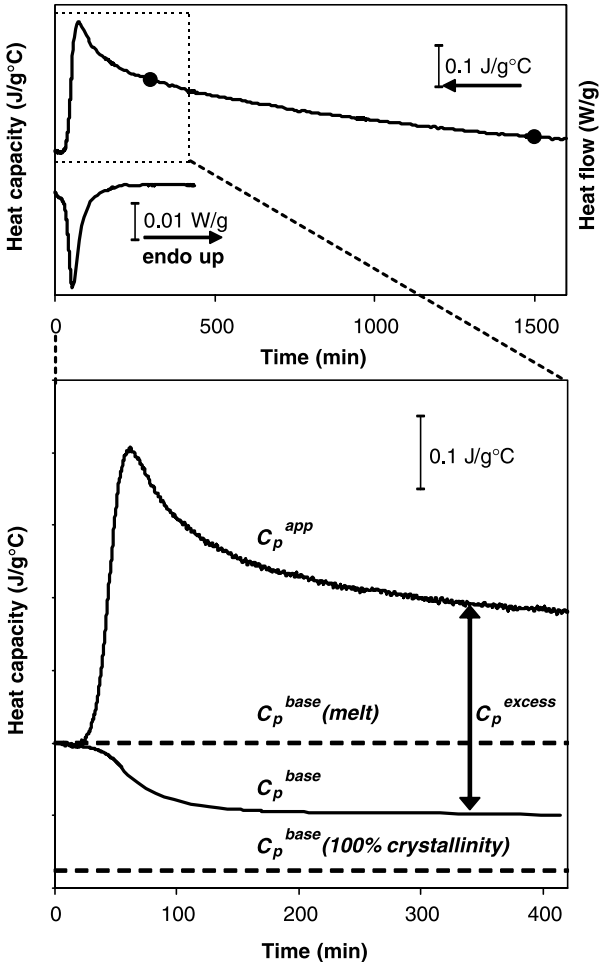

Fig. 6. Experimentally recorded MTDSC trace for the quasi-isothermal crystallization of poly(amide) 6 at 210 °C, showing the nomenclature for the different considered heat capacity levels (● indicate intervals used for time-domain analysis of Fig. 7).

the crystallinity at 210 °C, as crystallization is still occurring well after 1500 min (Fig. 5).

The long-term decrease in C_p^{app} ('slow' process on the timescale of the modulation) corresponds fairly well to the increase in melting enthalpy. This evolution in C_p^{app} describes a slow ongoing process of additional crystallization, along with crystal perfectioning (Figs. 4 and 5). Therefore, the decrease in C_p^{app} can be attributed to an equal decrease in C_p^{base} due to crystallization. This suggests that the magnitude of C_p^{excess} remains constant during the quasi-isothermal experiment.

3.2.3. *Time domain analysis of the 'fast' reversible process*

The origin of C_p^{app} and C_p^{excess} can be analyzed quantitatively by considering the raw modulated heat flow signal as a function of time (time domain analysis [13,33]). This approach has previously been applied to phase separation in polymer/water systems [13,15].

A time domain analysis of the raw MTDSC signals has been applied to the quasi-isothermal crystallization of the

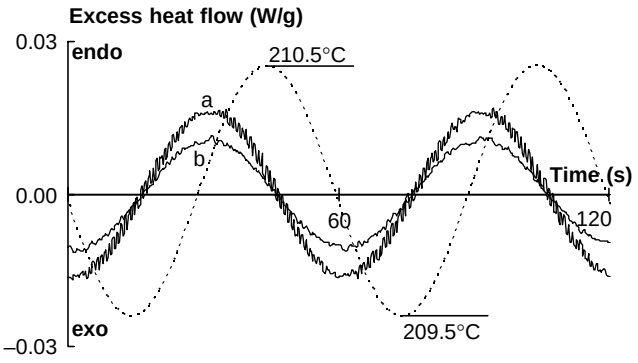

Fig. 7. The reversible excess heat flow at selected times showing the time-evolution: two modulation cycles after 300 (a) and 1500 min (b) of quasi-isothermal crystallization (indicated by dots in Fig. 6). The dashed line shows the temperature profile.

nanocomposites. In Fig. 7 an example is shown based on the results of Fig. 6. A sinusoidal excess heat flow is always observed (measured modulated heat flow minus the cyclic heat flow corresponding to C_p^{base}). After short crystallization times, when the crystallization exotherm is still seen in the non-reversing heat flow and a maximum is found in C_p^{app}, the excess heat flow is either totally or mainly exothermic (not shown in Fig. 7). This is due to the crystallization of poly(amide) 6 as a dominating irreversible process. After longer times, when the non-reversing heat flow is already at baseline level, exo and endothermic excess heat flows counterbalance each other (Fig. 7(a) and (b)), indicating that a reversible crystallization/melting situation is attained, which persists under these crystallization and modulation conditions, even after crystallization times as long as 8000 min. The excess heat flow is exothermic during a cooling segment (i.e. crystallization) and endothermic during a heating segment (i.e. melting).

A reliable quantitative analysis of the excess heat flows is difficult, mainly due to their small absolute values giving rise to enthalpies of crystallization and melting of ca. 0.3–0.4 J/g per half modulation cycle (compared to a crystallization enthalpy of 190 J/g for 100% crystalline poly(amide) 6 [32]). Nevertheless, the time domain analysis and C_p^{excess} allow a qualitative and comparative study and a physical/chemical interpretation for the phenomena playing a role in the interphase region of the different polymer/clay nanocomposites.

3.3. Influence of surfactant type

The origin of C_p^{excess} is the reversible melting and crystallization at the interface between the crystal edges and the polymer melt. In general, the magnitude of C_p^{excess} depends on the amount of heat exchanged within one temperature modulation cycle, which is determined by (i) the segmental mobility of the crystallizable chains and, hence, their crystallization rate, (ii) the amount of interface between the crystalline phase and the amorphous melt, and (iii) the enthalpy of crystallization/melting per unit of crystal-type involved in the reversible process. These three factors may influence C_p^{excess} of the poly(amide) 6/clay nanocomposites to a different extent, depending on the temperature modulation conditions (i.e. amplitude and/or frequency of the cyclic perturbation) and on the nature and amount of the (organo)clay used. The third factor can be rejected, however, as it has been reported that the heats of fusion of α- and γ-crystalline poly(amide) 6 are nearly identical [17].

3.3.1. Effect of modulation amplitude

In the first stages of quasi-isothermal crystallization, the crystallization kinetics do depend upon the amplitude of temperature modulation, because a different amplitude also implies a different supercooling and, hence, a different crystallization rate during each modulation cycle. For this reason C_p^{excess} will not be compared in the early stages of crystallization, at least not before the exothermicity in the non-reversing heat flow has disappeared.

In a later stage of quasi-isothermal crystallization, no change in C_p^{app} and, hence, in C_p^{excess} is observed on varying the amplitude of temperature modulation between 0.1 and 1 °C for poly(amide) 6 (Fig. 8). This is in agreement with non-isothermal experiments on poly(caprolactone) in the melting region [34]. In the case of filled poly(amide) 6 the situation is similar, as shown in Fig. 8 for 5 vol.% of neat clay.

These observations indicate that the amount of polymeric material taking part in the reversible process is not governed by the temperature modulation amplitude.

3.3.2. Effect of modulation frequency

A necessary condition for the observation of an excess contribution in the heat capacity is that the characteristic timescale of the reversible process is much shorter than or at least comparable to that of the imposed temperature modulation. The timescale of the reversible crystallization/melting process can become larger than that of the temperature modulation due to a restricted mobility of the chain segments of the crystallizable polymer matrix. In that case, the

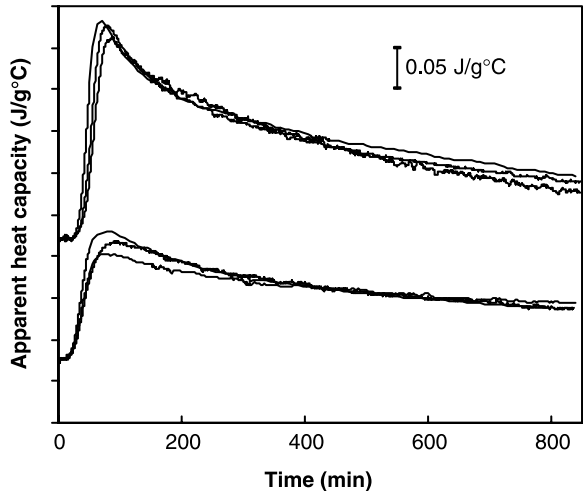

Fig. 8. Apparent heat capacity for the quasi-isothermal crystallization of poly(amide) 6 (upper three traces) and a nanocomposite with 5 vol.% of neat clay (lower three traces) at modulation amplitudes of 0.1, 0.5 and 1 °C and a period of 60 s (traces shifted for better comprehension).

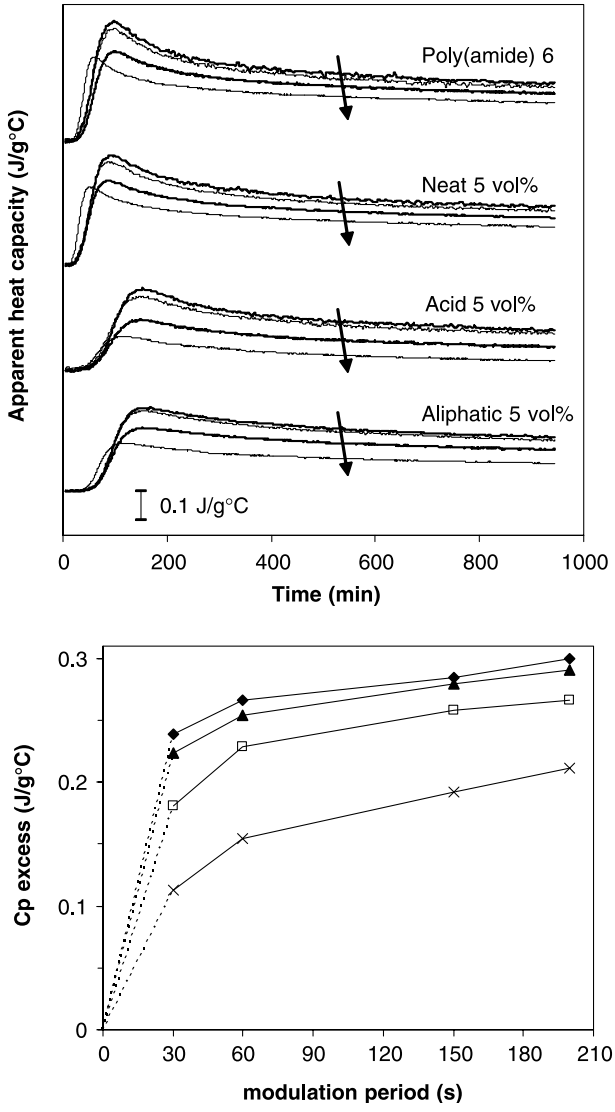

Fig. 9. (a) Apparent heat capacity during quasi-isothermal crystallization of poly(amide) 6 and different nanocomposites at modulation amplitude of 0.5 °C and periods of 200, 150, 60 and 30 s (arrows indicate decreasing periods); traces shifted vertically for different systems. (b) C_p^{excess}, calculated according to definitions in Fig. 6, as a function of modulation period for the experiments shown in (a); symbols as in Fig. 5.

magnitude of C_p^{excess} will decrease or might even vanish completely. The influence of a reduced segmental mobility on the lowering of the crystallization/melting rate, and as such on the decrease of C_p^{excess}, can be investigated by varying the modulation frequency.

As can be seen in Fig. 9(a), C_p^{excess} strongly depends on the imposed modulation period, longer periods yielding a larger C_p^{excess}, as also observed in [34]. This frequency dependency indicates that—in the frequency range accessible in MTDSC—not all of the potentially addressed polymer material does effectively take part in the reversible process. This is especially the case at the highest imposable frequencies (or shortest periods), where only a small portion of the crystallizable material is able to participate. Fig. 9(b) shows how C_p^{excess} depends on the modulation period for the different systems investigated. C_p^{excess} is calculated according to the definition from Fig. 6 and taking the organoclay loading into account. In the case of unfilled poly(amide) 6, a plateau-like value is fairly rapidly attained, whereas this evolution is more progressive for clay-filled poly(amide) 6. The slowest evolution towards a plateau value of C_p^{excess} at low frequencies is observed for nanocomposites based on acid-treated clay. It is, therefore, concluded that the chain segment mobility and hence the rate of crystallization/melting of part of the crystallizable polymer is decreased by the presence of clay, especially by the acid-treated clay.

3.3.3. Effect of surfactant type and clay loading

Using the same modulation conditions, i.e. the same modulation amplitude and period (e.g. ± 0.5 °C/60 s), the effect of the surfactant type and the clay loading can be investigated. Fig. 10 clearly shows that C_p^{app}, and hence the equilibrium excess heat capacity, depend on the type of surfactant (as could already be noticed in Fig. 9(b)). For samples based on neat clay, a clear dependency on clay loading is also observed, whereas for treated clays C_p^{app} (C_p^{excess}) is independent of the loading (between 1 and 10 vol.%). The inorganic barrier does not prevent the reversible crystallization/melting process, but in all nanocomposites C_p^{excess} is smaller than in the pure poly(amide) 6. This effect of surfactant type is interpreted in terms of loss of chain segment mobility in the vicinity of the clay, caused by specific interactions between the polymer chains and the clay platelets. As the polymer/clay interphase in nanocomposites constitutes a large fraction of the polymer matrix, due to the exfoliated or at least intercalated morphology of the dispersed clay, this region of reduced segmental mobility is influencing C_p^{excess} to a large extent. The magnitude of the decrease of C_p^{excess} depends on the interfacial interaction between matrix and filler: the stronger the interfacial interaction, the lower C_p^{excess} for a given clay loading. In addition, the stronger matrix–filler interaction and the higher loss of segmental mobility when using treated clays is also evidenced by the more pronounced frequency effect depicted in Fig. 9(b).

Note that the term ‘interfacial interaction’ is used in relation to chain segment mobility, while ‘interaction strength’ is avoided in this respect and will be solely reserved to describe the mechanical properties of the nanocomposites.

Obviously, the interfacial interaction between poly(amide) 6 and the acid and aliphatic treated clays is better than between poly(amide) and untreated clay (Fig. 10). The main interaction probably occurs with the ammonium head-groups of the surfactants, and the introduction of additional acid functional groups as in the ω-amino acid does not seem to further reduce C_p^{excess} to a large extent.

3.3.4. The ‘fast’ reversible process: relation with γ-type crystals

As already indicated, γ-type crystals are promoted by a restricted mobility of the poly(amide) 6 chain segments [19,20]. As the segmental mobility of the crystallizable chains is directly related to the magnitude of C_p^{excess}, a link between

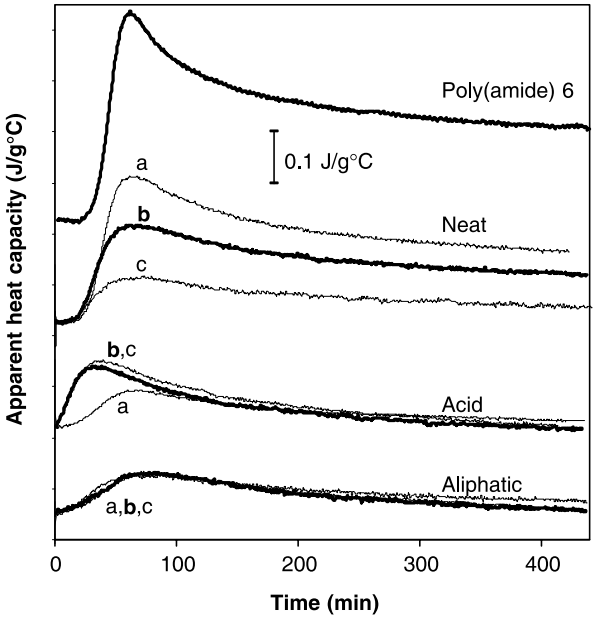

Fig. 10. Apparent heat capacity as measured during the quasi-isothermal crystallization of poly(amide) 6 and different nanocomposites with clay loadings of 1 (a), 5 (b) and 10 vol.% (c); traces shifted vertically for different systems.

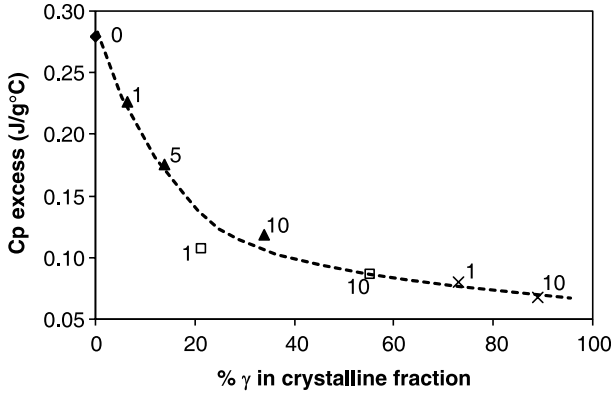

Fig. 11. Relationship between C_p^{excess} and the percentage of γ-crystals in the crystalline fraction. C_p^{excess} is measured by means of MTDSC during quasi-isothermal crystallization and the amount of γ-crystals is determined from WAXS experiments on isothermally crystallized samples. Each data point represents a different type of nanocomposite (symbols as in Fig. 5; loadings indicated). The dashed line is a guideline to the eye.

C_p^{excess} and the percentage of γ-type crystals is expected. Fig. 11 shows the relationship between the magnitude of C_p^{excess} (calculated from Fig. 10, according to the definition from Fig. 6 and taking the organoclay loading into account) and the amount of γ-phase in the crystalline fraction (determined from the WAXS patterns of Fig. 3, which is more reliable than using the calorimetric data in the melting region of Fig. 1). For nanocomposites based on neat clay, C_p^{excess} decreases with at least a factor 2 up to ca. 30% of γ-type crystals. The decrease is almost linear with increasing amount of clay. This proportionality is not found in the case of acid and aliphatic clays. For these samples, the drop in C_p^{excess} is high for low clay loadings of 1 vol.%, but a further decrease in C_p^{excess} for high clay loadings is clearly less pronounced. The acid clay gives the highest decrease in C_p^{excess}, in combination with the highest γ-fraction, up to 90%.

Not only the reduced chain mobility, caused by the poly(amide) 6–clay interaction, is determining the relative amounts of α- and γ-type crystals. The type of interaction, governed by the surface modification of the clay, is also important. Not all types of interaction do lead to crystallization in the γ-form, as out-of-plane bending of hydrogen bonds is not always involved. In this respect, the binding between poly(amide) 6 and the silica tetrahedrons of montmorillonite might be rather ineffective, as attested by the relatively low amount of γ-type crystals in nanocomposites based on neat clay. Increasing the clay loading decreases C_p^{excess}, as the number of amide functional groups bent out of the plane of the poly(amide) sheets is increasing and more poly(amide) becomes part of an interphase forming at the inorganic surface. In contrast, the specific interactions with the surfactant molecules (and mainly with their ammonium head-groups), seem to be effective enough to limit the reversible process that causes C_p^{excess}, and this already for a loading as low as 1 vol.% (Fig. 11). Increasing the amount of acid- or aliphatic-modified clay does not further reduce C_p^{excess} under the modulation conditions used, but further increases the fraction of γ-type crystals by the formation of out-of-plane hydrogen bonds. The influence of surfactant type and the absence of a straightforward and unique dependency on filler loading can be explained in terms of sample morphology, as discussed in the following section.

3.4. Interphase model

The quasi-isothermal crystallization behavior of poly(amide) 6/clay nanocomposites yields information on the molecular dynamics of the polymer in the presence of clay. The results obtained by means of MTDSC, along with WAXS information on the crystal structure, allow us to propose an interphase model for these nanocomposite materials, which is an extension of a model proposed earlier [35].

3.4.1. Poly(amide) 6/clay interphase

The interphase model is schematically represented in Fig. 12. Clay acts as a nucleating agent for the crystallization, and it has been reported that, at high temperatures, the γ-crystalline fraction is already formed in the early stages of crystallization [31]. It seems reasonable that the γ-type crystals form close to the clay platelets, due to the interaction between poly(amide) 6 and (organo)clay. Crystals of the α-type remain present in the nanocomposites, but they are located further away from the clay platelets, and can be considered as part of a semi-crystalline bulk-like phase, with poly(amide) chains hardly influenced by the presence of clay. The distance over which the γ-crystalline interphase and the bulk-like zone extend depends on the interfacial interaction between polymer and clay. For acid and aliphatic clay the amount of γ-crystalline material is already high at a loading of 1 vol.%.

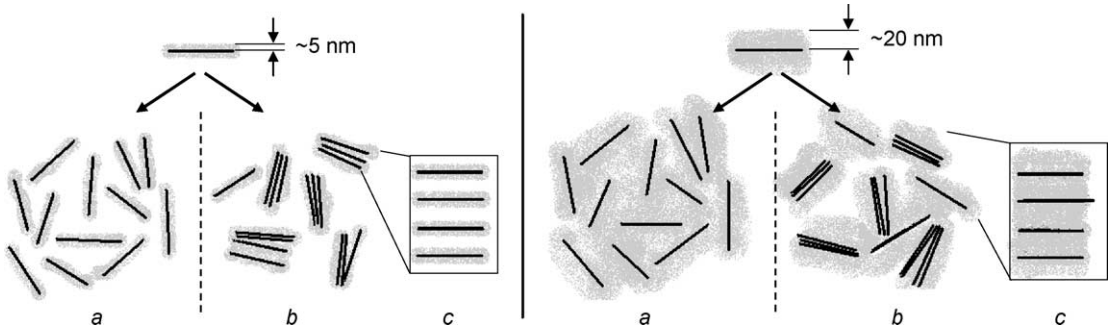

Fig. 12. Proposed structure model for poly(amide) 6 filled with neat clay (left, a–c) and acid clay (right, a–c). The grey shaded area around the clay platelets (black lines) represents a polymer fraction with reduced segmental mobility, with an extent depending on interfacial interaction. When the average inter-particle distance is large (low loading and fully exfoliated morphology), this layer of immobilized material can build up throughout the whole sample (a). At higher clay loading and/or incomplete exfoliation (b), the layer of immobilized polymer chains (per platelet) still reaches its maximum thickness for neat clay (c, left), but becomes limited to the inter-particle distance for acid clay (c, right).

A thick layer of γ-crystals exists around each individual platelet, associated with a high reduction in segmental mobility and decrease in C_p^{excess} (Fig. 11). With increasing clay loading, the γ-crystalline fraction still increases, but a proportional decrease in C_p^{excess} is not observed (Fig. 11). A possible explanation is that, at high loadings, the average distance between the clay platelets decreases considerably (the structure even tends to become intercalated). The layer of immobilized polymer chains (per platelet) no longer reaches its maximum thickness, but becomes limited to the space in between the clay platelets (Fig. 12). This situation does not occur to such an extent with neat clay, as the thickness of the γ-crystalline layer around each platelet is limited compared to the average inter-particle distance (Fig. 12). Therefore, the difference between an exfoliated and intercalated morphology has little implication on the amount of polymer affected (immobilized) by the presence of neat clay (Fig. 11).

The observations on the glass transition temperature, T_g, also fit in the proposed model. If the amorphous polymer fraction, or part of it, would interact with the filler, this could lead to a delayed mobility and eventually eliminate any cooperative motion in the polymer chains. In the former case, an amorphous fraction with a raised T_g would appear. In the latter case, the amorphous polymer fraction might even become undetectable. None of the nanocomposites showed an increase in the position of T_g, nor in the heat capacity change, ΔC_p, at T_g (Fig. 2). The 25% decrease in crystallinity in the acid nanocomposite (Fig. 5) should accordingly result in an increase of the amorphous fraction by 10% (on a basis of a 40% overall crystallinity). This effect is not noticed (Fig. 2), indicating that an undetectable (immobilized) amorphous fraction of up to ca. 10% is present, which is located close to the clay platelets. In this respect it is worth noting that the amount of immobilized polymer is almost independent of the clay loading in the investigated samples (Fig. 2), as was also the case for the reduction in C_p^{excess} for nanocomposites based on acid-treated clay (see discussion on Figs. 10–12). This suggests a common origin for the decrease in C_p^{excess} and ΔC_p, i.e. the interactions between the matrix and the organoclay, reducing the mobility of part of the polymer, hence rendering its amorphous part undetectable. The measured glass transition might, therefore, be assigned to an amorphous fraction located further away from the clay, where interactions are less prominent. This bulk-like region of the matrix has a semi-crystalline morphology with α-type crystals. These MTDSC findings on the amorphous poly(amide) fraction are in agreement with pressure–volume–temperature data obtained for an analogous series of nanocomposites [36], as well as with ΔC_p measurements at T_g for fully amorphous poly(styrene)/clay nanocomposites [37].

Note that a small additional crystalline fraction of the modifier of the aliphatic-treated nanocomposites might be located in intercalated clay regions, which explains why it is still able to melt and crystallize far below the melting region and even below the T_g of poly(amide) 6 (Fig. 2) [38].

3.4.2. The link with mechanical properties?

Even though the interphase model is based on the measurement of phenomena taking place on a nanometer level, it might also be in agreement with the macroscopic mechanical properties of the nanostructured material (reported in Ref. [6]).

The MTDSC results have been interpreted in terms of interactions between polymer and clay and restrictions of chain segment mobility in the vicinity of the clay platelets. The interactions evidenced by MTDSC will also influence the mechanical behavior of the nanocomposites. However, the different types of interactions have different implications for the mechanical behavior of the materials. Mechanical 'interaction strength' is not necessarily equivalent to 'interfacial interaction' defined in relation to segmental mobility. Some interactions are strong and improve mechanical strength, for instance the polar interaction between poly(amide) and neat clay [6,39]. Other interactions, such as the ion–dipole interaction between poly(amide) and surfactant molecules, are effective to reduce the segmental mobility and promote the formation of γ-crystals, but are not necessarily beneficial to the mechanical properties [6,39].

In addition, a straightforward link between thermal and mechanical properties cannot be easily drawn because the former only weakly account for the sample morphology, i.e. the degree of clay exfoliation vs. intercalation, which is

a crucial parameter towards improvement of mechanical properties [1].

4. Conclusions

The melting and crystallization behavior as well as the glass transition region of clay-reinforced poly(amide) 6 nanocomposites were studied using modulated temperature differential scanning calorimetry. The use of this thermal analysis information, along with confirmation from X-ray scattering experiments, enables the investigation of the effect of interactions between organic polymer and inorganic reinforcement in the studied nanocomposites.

Clays with different organic modifications have been tested in poly(amide) 6 nanocomposites to fine-tune the interfacial interaction between polymer matrix and reinforcing particles.

It was demonstrated, through the measurement of an excess heat capacity during quasi-isothermal crystallization, that the presence of surfactant induces a more effective interaction between the poly(amide) 6 matrix and the clay. This has severe consequences on the crystallization behavior of the nanocomposites, and especially on the mobility of polymer chain segments in the vicinity of the clay platelets. This, in turn, is believed to cause the formation of a γ-type crystal structure in the interphase region. The amount of γ-type crystals instead of the α-form depends on the organic treatment and on the amount of clay.

It was proven that the observed excess in the heat capacity is linked to phenomena taking place on a nanometer-scale. It can be directly used for the detection of interfacial interaction between matrix and reinforcement in the nanocomposite materials. We have proposed to use the magnitude of the excess heat capacity as a direct measure for this interfacial interaction.

These nano-scale processes, driven by the physical and chemical nature of the (organically modified) reinforcement, affect the final macroscopic properties of the nanocomposites, such as thermal and mechanical properties. The link between the MTDSC results and the mechanical properties, however, is not straightforward.

A simple interphase model was presented for the investigated nanomaterials. We have shown that the type of surfactant used to modify the clay is the key factor. It determines the type of interfacial interaction and, as such, the segmental mobility of the polymer in the interphase region, where both the crystalline and amorphous fractions are affected.

Acknowledgements

The work of H.E. Miltner and G. Van Assche was supported by a grant of the Fund for Scientific Research-Flanders (F.W.O.-Vlaanderen).

A. Pozsgay and B. Pukánszky kindly acknowledge the National Scientific Research Fund for financial support (OTKA Grant No. T043517).

The authors are grateful to Prof M.-P. Delplancke (Université Libre de Bruxelles-Service de Chimie Industrielle) for the X-ray experiments.

References

[1] Alexandre M, Dubois P. Mater Sci Eng, R 2000;28:1–63.
[2] Giannelis EP. Adv Mater 1996;8:29–35.
[3] Ray SS, Okamoto M. Prog Polym Sci 2003;28:1539–641.
[4] van Es M. Polymer–clay nanocomposites: the importance of particle dimensions. PhD Thesis. TU Delft, The Netherlands; 2001.
[5] Dennis HR, Hunter DL, Chang D, Kim S, White JL, Cho JW, et al. Polymer 2001;42:9513–22.
[6] Rácz L, Pukánszky Jr B, Pozsgay A, Pukánszky B. Prog Colloid Polym Sci 2004;125:96–102.
[7] Reading M, Luget A, Wilson R. Thermochim Acta 1994;238:295–307.
[8] Wunderlich B, Jin Y, Boller A. Thermochim Acta 1994;238:277–93.
[9] Ishikiriyama K, Wunderlich B. J Polym Sci, Part B: Polym Phys 1997;35:1877–86.
[10] Minakov AA, Schick C. Thermochim Acta 1999;330:109–19.
[11] Dreezen G, Groeninckx G, Swier S, Van Mele B. Polymer 2001;42:1449–59.
[12] Swier S, Pieters R, Van Mele B. Polymer 2002;43:3611–20.
[13] Swier S, Van Durme K, Van Mele B. J Polym Sci, Part B: Polym Phys; 2003.
[14] Van Durme K, Verbrugghe S, Du Prez F, Van Mele B. Macromolecules 2004;37:1054–61.
[15] Van Durme K, Van Assche G, Van Mele B. Macromolecules 2004;37:9596–605.
[16] Fornes TD, Yoon PJ, Hunter DL, Keskkula H, Paul DR. Polymer 2002;43:5915–33.
[17] Fornes TD, Paul DR. Polymer 2003;44:3945–61.
[18] Xenopoulos A, Clark ES. Physical structure. In: Kohan MI, editor. Nylon plastics handbook. Munich: Hanser Publishers; 1995.
[19] Mathias LJ, Davis RD, Jarrett WL. Macromolecules 1999;32:7958–60.
[20] Lincoln DM, Vaia RA, Wang Z-G, Hsiao BS, Krishnamoorti R. Polymer 2001;42:9975–85.
[21] Kojima Y, Usuki A, Kawasumi M, Okada A, Kurauchi T, Kamigaito O, et al. J Polym Sci, Part B: Polym Phys 1994;32:625–30.
[22] Wu Q, Liu X, Berglund LA. Polymer 2002;43:2445–9.
[23] Lincoln DM, Vaia RA, Wang Z-G, Hsiao BS. Polymer 2001;42:1621–31.
[24] Liu X, Wu Q. Eur Polym J 2002;38:1383–9.
[25] Kojima Y, Matsuoka T, Takahashi H, Kurauchi T. J Appl Polym Sci 1994;51:683–7.
[26] Devaux E, Bourbigot S, El Arachi A. J Appl Polym Sci 2002;86:2416–23.
[27] Vaia RA, Sauer BB, Tse OK, Giannelis EP. J Polym Sci, Part B: Polym Phys 1997;35:59–67.
[28] Inan G, Celik C, Patra PK. NATAS. Conference Proceedings; 2003.
[29] Zax DB, Yang D-K, Santos RA, Hegemann H, Giannelis EP, Manias E. J Chem Phys 2000;112:2945–51.
[30] Krishnamoorti R, Vaia RA, Giannelis EP. Chem Mater 1996;8:1728–34.
[31] Lincoln DM, Vaia RA, Krishnamoorti R. Macromolecules 2004;37:4554–61.
[32] Inoue M. J Polym Sci, Part A: Gen Pap 1963;1:2697–709.
[33] Androsch R, Wunderlich B. Macromolecules 1999;32:7238–47.
[34] Merzlyakov M, Wurm A, Zorzut M, Schick C. J Macromol Sci, Phys 1999;B38:1045–54.
[35] Maiti P, Okamoto M. Macromol Mater Eng 2003;288:440–5.
[36] Utracki LA, Simha R, Garcia-Rejon A. Macromolecules 2003;36:2114–21.
[37] Li YQ, Ishida H. Macromolecules 2005;38:6513–9.
[38] Li YQ, Ishida H. Chem Mater 2002;14:1398–404.
[39] Fermeglia M, Ferrone M, Pricl S. Fluid Phase Equilib 2003;212:315–29.